


Letter

# A Synergetic Approach to Burned Area Mapping Using Maximum Entropy Modeling Trained with Hyperspectral Data and VIIRS Hotspots

Alfonso Fernández-Manso <sup>1</sup> and Carmen Quintano <sup>2,3,\*</sup> 

<sup>1</sup> Agrarian Science and Engineering Department, University of León, Av. Astorga s/n. 24400-Ponferrada, Spain; alfonso.manso@unileon.es

<sup>2</sup> Electronic Technology Department, University of Valladolid, Paseo del Cauce, 59, 47011-Valladolid, Spain

<sup>3</sup> Sustainable Forest Management Research Institute, University of Valladolid-Spanish National Institute for Agricultural and Food Research and Technology, C/Francisco Mendizábal s/n, 47014 Valladolid, Spain

\* Correspondence: carmen.quintano@uva.es

Received: 4 February 2020; Accepted: 5 March 2020; Published: 6 March 2020



**Abstract:** Southern European countries, particularly Spain, are greatly affected by forest fires each year. Quantification of burned area is essential to assess wildfire consequences (both ecological and socioeconomic) and to support decision making in land management. Our study proposed a new synergetic approach based on hotspots and reflectance data to map burned areas from remote sensing data in Mediterranean countries. It was based on a widely used species distribution modeling algorithm, in particular the Maximum Entropy (MaxEnt) one-class classifier. Additionally, MaxEnt identifies variables with the highest contribution to the final model. MaxEnt was trained with hyperspectral indexes (from Earth-Observing One (EO-1) Hyperion data) and hotspot information (from Visible Infrared Imaging Radiometer Suite Near Real-Time 375 m active fire product). Official fire perimeter measurements by Global Positioning System acted as a ground reference. A highly accurate burned area estimation (overall accuracy = 0.99%) was obtained, and the indexes which most contributed to identifying burned areas included Simple Ratio (SR), Red Edge Normalized Difference Vegetation Index (NDVI<sub>750</sub>), Normalized Difference Water Index (NDWI), Plant Senescence Reflectance Index (PSRI), and Normalized Burn Ratio (NBR). We concluded that the presented methodology enables accurate burned area mapping in Mediterranean ecosystems and may easily be automated and generalized to other ecosystems and satellite sensors.

**Keywords:** EO-1 Hyperion; burned area; spectral indexes; Mediterranean ecosystems; MaxEnt; VIIRS hotspots

## 1. Introduction

Wildfires are natural disturbances in many ecosystems [1], particularly Mediterranean ones. At the regional / local scale they can cause serious socio-economic problems affecting property and lives [2]. In that case, post-fire damage maps may provide crucial information for legal purposes (land use change, illegal burning, and insurance costs) [3]. In addition, an adequate post-fire management policy that prevents soil losses and promotes vegetation regeneration can only be based on accurate fire damage maps (burned area / burn severity) [4]. Nowadays, reliable burned area estimates at all scales are obtained using remote sensing data and techniques [5]. In particular, hyperspectral remote sensing of fire damage enables the accurate discrimination and quantification of burned areas, burn severity, and vegetation recovery [5]. Hyperspectral imagery has been successfully used in different fire studies [6,7]; the Hyperion sensor onboard the Earth-Observing One (EO-1) platform provided data that have been successfully utilized for fire detection [8,9] and burn severity mapping [10–12].

Red, near infrared (NIR), and short-wave infrared (SWIR) spectral bands have proved their usefulness in fire damage studies, providing an accurate discrimination of burned areas [13]. Two spectral indices based on these wavelengths, the Normalized Difference Vegetation Index (NDVI) and, more recently, the Normalized Burn Ratio (NBR) are considered standard references for burned area mapping at the local scale [13]. However, Red Edge wavelength-based indices (as Chlorophyll Index Red Edge (CI<sub>re</sub>) [14], Modified Simple Ratio Red Edge narrow (MSR<sub>ren</sub>) [15], or Red Edge Normalized Difference Vegetation Index (NDVI<sub>750</sub>) [16]) are also revealing their suitability for fire damage mapping [15,17–19].

Synergetic approaches integrating data from different sensors and wavelengths are proving their strengths in mapping burned areas [2]. Among the most synergetic approaches, the combination of hotspots (from thermal bands) and the changes (due to fires) reflected from visible, NIR, and SWIR spectral regions are outstanding [20,21]. Changes in thermal bands due to fire enable a correct identification of active fires, which complements the discrimination of burned area based on changes in visible, NIR, and SWIR bands [2]. In this context, we present a new synergetic approach for mapping burned areas based on a combination of Hyperion EO-1 hyperspectral indexes and hotspots from the Near Real-Time (NRT) Suomi National Polar-orbiting Partnership (S-NPP) / Visible Infrared Imaging Radiometer Suite (VIIRS) 375 m active fire product (VNP14IMGTDL\_NRT) [22].

The present study uses a Maximum Entropy one-class classifier (MaxEnt) [23] to model and map burned area. MaxEnt estimates the probability of the target area presence based on the combination of presence-only samples of this class and different variables (called covariates) [24]. MaxEnt has been commonly used as a model for species distributions [25–27], but it is being progressively used in remote sensing based applications as well [12,28,29]. Additionally, it has been successfully used to model fire occurrence [30,31] and burn severity [12,32]. Quintano et al. (2019) [30] used MaxEnt to estimate both burn severity and burned area from Sentinel-2 Multispectral Instrument (MSI) Multiple Endmember Spectral Mixture Analysis (MESMA) fraction images and post-fire Landsat 8 OLI LST images. The burned area estimate achieved an overall accuracy equal to 93%. To our knowledge, this is the only MaxEnt-based burned area study, despite MaxEnt's advantages over other classifiers: 1) MaxEnt is a non-parametric model; 2) MaxEnt is an attractive substitute for machine learning based classifiers, as only presence-only samples are needed to train it; and 3) its probabilistic output has physical meaning, making it easy to interpret [33].

In this context, our hypothesis is that burned areas can be considered the target distribution of MaxEnt and modeled with presence-only data, as we only have past fire occurrences available. Our work aims to validate a new and semi-automatic synergetic methodology to estimate accurately burned areas at the local scale based on the one-class classifier MaxEnt trained with hyperspectral EO-1 Hyperion indexes as covariates and VNP14IMGTDL\_NRT hotspots as presence-only data. The study was tested in a Mediterranean ecosystem.

## 2. Materials and Methods

### 2.1. Materials

The Carcaixent wildfire happened in central-eastern Spain (a Mediterranean climate) from 16 to 19 June 2016 (Figure 1). It burned an area of 2291 ha, which was covered primarily by shrubland dominated by sprouting species and forest dominated by Aleppo pine (*Pinus halepensis* L.) [34].

The burned area was estimated using a post-fire hyperspectral EO-1 Hyperion scene acquired on July 21, 2016. The solar zenith angle was 8 degrees, and cloud coverage was 10%–19%. VIIRS NRT 375 m active fire product (VNP14IMGTDL\_NRT) provided the presence-only data to train MaxEnt (in “.csv” format). The official fire perimeter was used as a ground reference to validate the model.

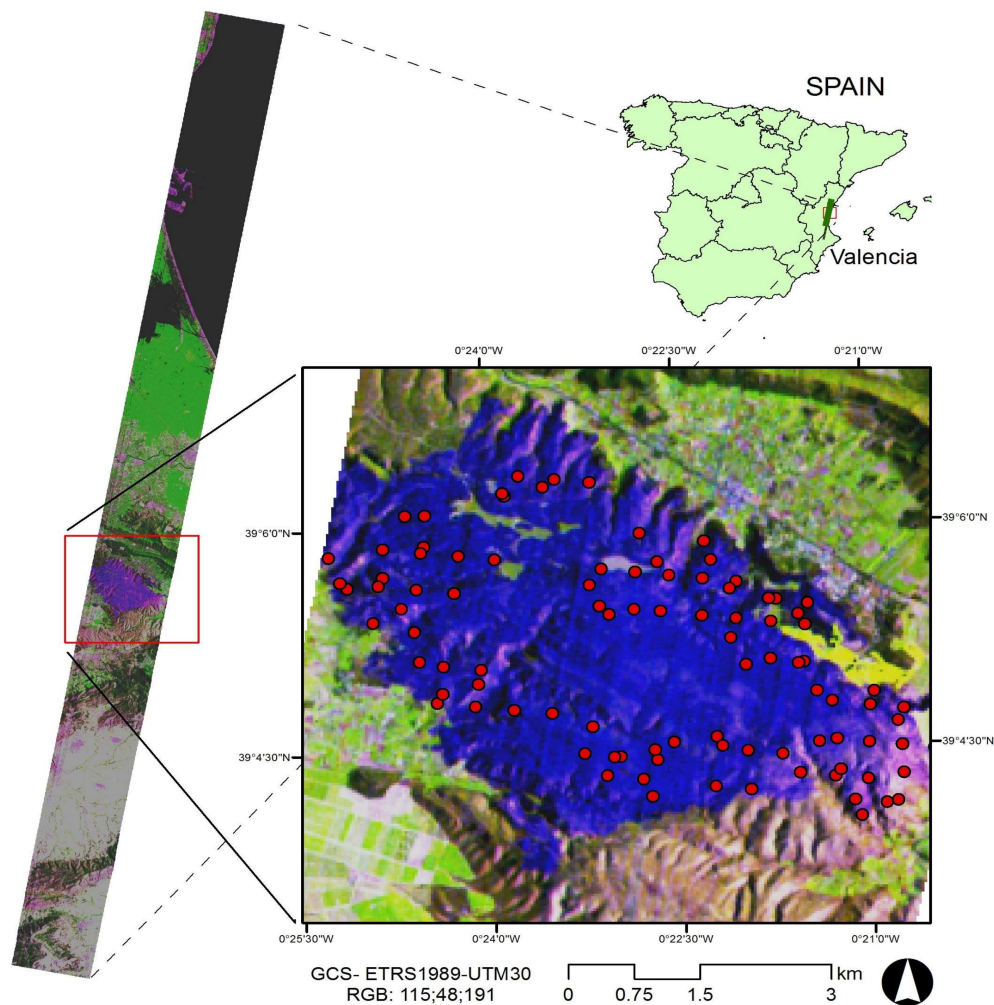


**Figure 1.** Study area. Earth-Observing One (EO-1) Hyperion color composition (RGB: 115:48:191) and fire hotspots from Visible Infrared Imaging Radiometer Suite Near Real-Time (VIIRS NRT) 375 m active fire product.

## 2.2. Methods

The EO-1 Hyperion data were delivered as a radiometric-, geometric-, and terrain-corrected image (L1T level). Bands that showed bad lines, striping, or very high noise were discarded. Thus, we kept 106 bands, covering the entire spectrum from 426 to 2395 nm. The Fast Line-of-sight Atmospheric Analysis of Hypercubes (FLAASH) algorithm allowed us to correct the data atmospherically and transform them to surface reflectance. Next, fourteen spectral indexes covering all wavelength ranges, and similar to those used in different burned area studies, were computed and grouped into five categories: 1) related to broadband greenness (NDVI [35], Simple Ratio (SR) [36], and Sum Green Index (SGI) [37]); 2) related to narrowband greenness (Red Edge Normalized Difference Vegetation Index (NDVI<sub>750</sub>) [16], Vogelmann Red Edge Index 1 (VOG1) [38], Red Edge Position Index (REPI) [39]); 3) related to canopy water content (Normalized Difference Water Index (NDWI) [40], Normalized Difference Infrared Index (NDII) [41], and Moisture Stress Index (MSI) [42]); 4) related to dry or senescent carbon (Normalized Difference Lignin Index (NDLI) [43] and Plant Senescence Reflectance Index (PSRI) [44]); and 5) related to light use efficiency (Photochemical Reflectance Index (PRI) [45] and Red Green Ratio Index (RGRI) [46]). In addition, NBR [47] was included as a reference (see Supplementary Material, Table S1).

MaxEnt software (version 3.4.1) [23,24] needs two types of input data: covariates (EO-1 Hyperion spectral indexes in our case) and georeferenced locations of presence-only training samples (94 hotspots

from VNP14IMGTDL\_NRT). As in previous studies [48,49], we used 75% of the samples to train MaxEnt, 25% for testing purposes, and 10 replicates with a repeated subsampling scheme. The rest of user-specified parameters were set to their default values. The MaxEnt output provided an estimate of the probability of burned area (target-class) presence. In addition, MaxEnt produced a percentage contribution table reflecting the model's gain with each feature included during the training process, which allowed us to rank the covariates' importance in the modeling process. Moreover, a receiver operating characteristic (ROC) analysis where area under the curve (AUC) [50] represents the model's capability to adequately predict presence (sensitivity) and absence (specificity) was provided by MaxEnt to evaluate the model. Finally, the continuous MaxEnt output was converted into a binary burned area map. Kappa statistics [51] were used to find the optimal threshold defined by MaxEnt. To compute the  $\kappa$  statistic, approximately 10% of the pixels of each class of interest (burned, unburned) were selected by stratified random sampling from the rasterized official fire perimeter to calculate an error matrix. User accuracy (UA), producer accuracy (PA), and overall accuracy (OA) were computed as well.

### 3. Results

From the MaxEnt percentage contribution table we could identify five hyperspectral indexes as the highest contributors to model the burned area: SR from the broadband greenness group, NDVI<sub>750</sub> from the narrowband greenness group, NDWI from the canopy water content group, PSRI from the dry or senescent carbon group, and NBR. Thus, the definitive model was implemented exclusively using these five indexes.

Table 1 summarizes the performance parameters of the modeling process. AUC values were always higher than 0.9, which indicated excellent model performance [52]. NBR, NDWI, and NDVI<sub>750</sub> contributed 80%, and the contributions of SR and particularly of PSRI were lower. Regarding the training gain, we noticed very small differences among the indexes, which indicated that all covariates contributed in a similar way to reaching a good fit to the training data. Regarding the test gain, which measures the contribution of the covariates to fit the model to the training data, and showing whether the predictive performance improves when the corresponding covariate is used alone or excluded, we found the same pattern. No important differences among the indexes were found, which denotes that all indexes may generalize comparably. Similarly, no greatly significant differences were found regarding AUC values when each covariate was used alone or excluded. Taking into account the test gain values is important if the goal is to transfer the model, for example by applying the defined model to indexes from a future remotely sensed image in order to estimate a future burned area. In our study, no one index would make the model much less transferable than another index.

Figure 2 displays the ROC curves for the best model and the average model, suggesting in both cases an excellent performance. Finally, Figure 3 (left) shows the MaxEnt output that represents the suitability surface for burned-class occurrence. We classified it using the different thresholds suggested by MaxEnt and applied a post-classification 4x4 majority filter. The threshold that maximized training sensitivity plus specificity was the threshold that maximized the  $\kappa$  statistic, which was  $\kappa = 0.96$ , UA = 98%, PA = 97%, and OA = 99% (see Supplementary Material, Tables S2 and S3). Figure 3 (right) displays the definitive burned area map. The high value of the  $\kappa$  statistic is remarkable. From the error matrix (Tables S2 and S3) we observed that UAs from both classes were quite similar (98%), suggesting very small commission errors. In fact, in Figure 3 (right) we noticed there were almost no burned area estimates outside the fire perimeter. Regarding PA, the unburned class reached PA = 99%. However, the PA of the burned area was 95%, indicating a small omission error in this class.

Table 1. Summary of parameters of modeling process.

Summary of Parameters of Modeling Process (Average Model)					
	#Samples	Gain	AUC	AUC Standard Deviation	
Training	70	2.1936	0.9555		
Test	24	2.177	0.9547	0.0061	
Percentage of Contribution of Selected Covariates (%) (Average Model)					
NBR	NDWI	NDVI <sub>750</sub>	SR	PSRI	
32.4314	20.4293	19.3503	16.5978	11.1911	
Training Gain (Average Model)					
	NBR	NDWI	NDVI <sub>750</sub>	SR	PSRI
Without the covariate	2.0773	2.1036	2.1069	1.9733	2.1099
With only the covariate	1.2142	1.3437	1.4624	1.1222	1.4170
Test Gain (Average Model)					
	NBR	NDWI	NDVI <sub>750</sub>	SR	PSRI
Without the covariate	2.1460	2.1395	2.1657	2.0627	2.1528
With only the covariate	1.2093	1.5127	1.4618	1.1529	1.4525
AUC (Average Model)					
	NBR	NDWI	NDVI <sub>750</sub>	SR	PSRI
Without the covariate	0.9540	0.9537	0.9540	0.9519	0.9527
With only the covariate	0.8881	0.9191	0.9155	0.8816	0.9113

Average model: model whose parameters were obtained by averaging the parameters in each of the 10 replicates.

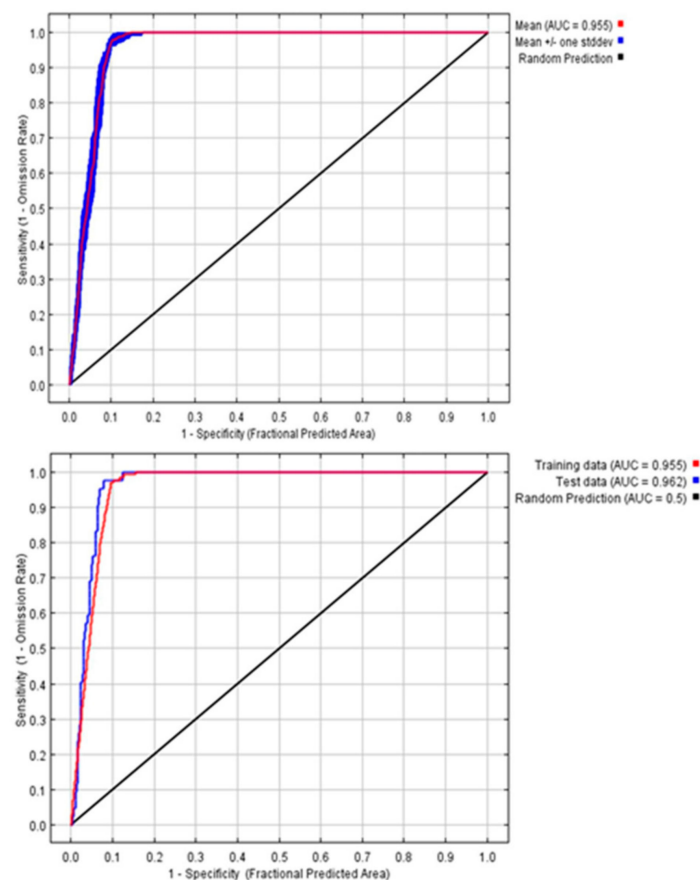
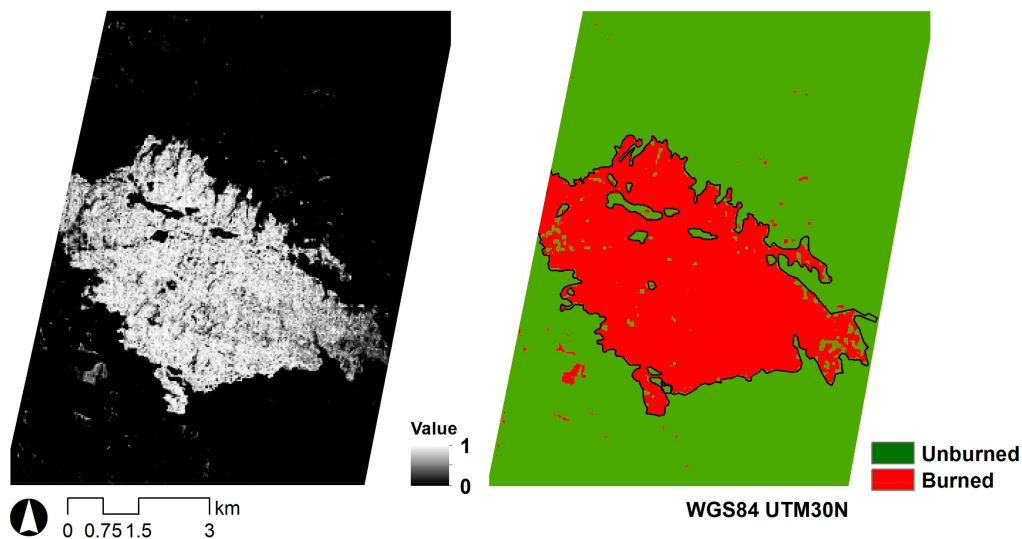


Figure 2. ROC curves. Upper: averaged model over 10 replicate runs; lower: best model.



**Figure 3.** Left: Maximum Entropy (MaxEnt) probability output (0: 0% probability; 1: 100% probability); right: burned area map.

#### 4. Discussion

NBR, the reference index based on NIR and SWIR, had the highest contribution to the model, followed by NDWI, a canopy water content index based on NIR and SWIR1, and NDVI<sub>750</sub>, a narrowband greenness index that included Red Edge wavelengths. SR, a broadband greenness index based on NIR and red had a lower contribution. Finally, PSRI, a dry or senescent carbon index including red, green, and Red Edge wavelengths, had the lowest contribution. Previous studies based on remote sensing sensors without Red Edge wavelengths (e.g., [4]) have already shown that red, NIR, and SWIR bands are the most adequate to identify burned areas. Fernández-Manso et al. [15], working with Sentinel-2 MSI data showed that Red Edge based indexes are appropriate to identify burned areas and discriminate burn severity levels. Red Edge Sentinel-2 MSI bands were also confirmed as the most suitable to detect burned areas, together with NIR and SWIR, by following research works [19,53]. Moreover, Red Edge bands have also been identified as appropriate to discriminate burned from unburned areas using UAV multispectral data [18]. Thus, our study agrees with previous studies and confirms that NIR, SWIR, Red Edge, and red are the wavelength ranges most useful to map burned areas.

Table 1 also showed that the burned area model was highly transferable (high and similar test gain and AUC values for the five input spectral indexes). In this way, NBR, NDWI, NDVI<sub>750</sub>, and SR (contributing more than 94%) could be computed with Sentinel-2 MSI data, which are more easily available than EO-1 Hyperion data. Though the spectral and spatial resolution are different, Sentinel-2 MSI spectral indices have already shown their suitability for discriminating burned areas [19,54,55]. Thus, we believe that the proposed methodology may be generalized using Sentinel-2 MSI data; however, we leave this test for future studies. Moreover, we are convinced that it may also be generalized using data from the upcoming space-borne hyperspectral missions as the recently launched Hyperspectral Precursor and Application Mission (PRISMA) hyperspectral sensor. In this study, we validated the methodology of a wildfire that happened in a Mediterranean ecosystem, but it may equally be extrapolated to other ecosystems, as it is not based on any ecosystem-dependent characteristic. Furthermore, it can be easily quasi-automated as there could be no human-dependent processes in the proposed method: 1) presence-only data are imported directly from VIIRS NRT hotspots using a “.csv” file; and 2) the conversion of the probability output into a binary burned area map could be done using the threshold suggested by MaxEnt that maximizes training sensitivity plus specificity, and that additionally maximized the  $\kappa$  statistic in our study. These generalizations will be evaluated in future research works.

Our research is an example of a more synergetic combination of hotspots from thermal bands and reflectance data covering red, Red Edge, NIR, and SWIR wavelengths. Since those synergetic approaches were first proposed [56,57], they have been employed to estimate burned area both at the regional and global scales. Among others, Tansey et al. [58] successfully mapped burned areas, combining hotspots and Landsat TM 7 data, and Rotteta et al. [59] combined hotspots and Sentinel 2 data. Moreover, the MCD64A1 product from NASA [21], and FireCCI50 from ESA [60] are based on that synergetic procedure.

MaxEnt only built a probability image of burned area, but depending on the specific needs, different burned area maps may be produced. That continuous suitability surface (or probability of occurrence map) is the most valuable information for forest managers, as they might select an appropriate threshold according to the project priorities [61,62]. Thus, the availability of continuous suitability surfaces as MaxEnt output constitutes one advantage over well-established classifiers [32,62].

## 5. Conclusions

Our study evaluated the use of a synergetic approach based on a distribution-modeling algorithm trained by hyperspectral indexes and hotspots to model and map burned areas. Thus, the presence-only samples to train MaxEnt were obtained from the hotspots identified in the Visible Infrared Imaging Radiometer Suite Near Real-Time 375 m active fire product. We examined the relative contribution on burned area modeling of different spectral indices that acted as covariates. In particular, NBR contributed 33%, NDVI 24%, NDVI<sub>750</sub> 23%, SR 14%, and PSRI only 6%. The three first covariates (NBR, NDWI, and NDVI<sub>750</sub>) added a percentage of contribution of 80%. Using the official fire perimeter measured by Global Positioning System as a ground reference, the burned area map reached a  $\kappa$  statistic value equal to 0.96, which indicates a high accuracy. Our results verified that a distribution model trained with hyperspectral indices covering red, Red Edge, NIR, and SWIR wavelengths provided an accurate burned area map in Mediterranean ecosystems. Moreover, MaxEnt provided a continuous suitability surface that was easy to interpret and had valuable information that enhanced the burned area map. Thus, the new proposed methodology may help forest managers to plan appropriate post-fire management strategies to reduce fire damage repercussions. Future research should evaluate this method at a larger scale, in different fire events, and compare it with other learning machine-based methods.

**Supplementary Materials:** The following are available online at <http://www.mdpi.com/2072-4292/12/5/858/s1>, Table S1: Spectral indexes, Table S2: Error matrix, Table S3: Accuracy parameters.

**Author Contributions:** Conceptualization, A.F.-M. and C.Q.; methodology, A.F.-M. and C.Q.; software, A.F.-M.; validation, A.F.-M. and C.Q.; writing—original draft preparation, C.Q.; writing—review and editing, A.F.-M. and C.Q. All authors have read and agreed to the published version of the manuscript.

**Funding:** Funding for this study was provided by the Spanish Ministry of Economy and Competitiveness (FIRESEVES project, AGL2017-86075-C2-1-R) and the Regional Government of Castile and León (SEFIRECYL project, LE001P17).

**Acknowledgments:** We acknowledge the use of VNP14IMGTDL\_NRT product from LANCE FIRMS operated by the NASA/GSFC/Earth Science Data and Information System (ESDIS) with funding provided by NASA/HQ.

**Conflicts of Interest:** The authors declare no conflicts of interest.

## References

1. Bowman, D.M.J.S.; Balch, J.K.; Artaxo, P.; Bond, W.J.; Carlson, J.M.; Cochrane, M.A.; D'Antonio, C.M.; Defries, R.S.; Doyle, J.C.; Harrison, S.P.; et al. Fire in the earth system. *Science* **2009**, *324*, 481–548. [[CrossRef](#)]
2. Chuvieco, E.; Mouillot, F.; Van der Werf, G.R.; San-Miguel, J.; Tanase, M.; Koutsias, N.; García, M.; Yebra, M.; Padilla, M.; Gitas, I.; et al. Historical background and current developments for mapping burned area from satellite Earth observation. *Remote Sens. Environ.* **2019**, *225*, 45–64. [[CrossRef](#)]

3. Mouillot, F.; Schultz, M.G.; Yue, C.; Cadule, P.; Tansey, K.; Ciais, P.; Chuvieco, E. Ten years of global burned area products from spaceborne remote sensing—A review: Analysis of user needs and recommendations for future developments. *Int. J. Appl. Earth Obs. Geoinf.* **2014**, *26*, 64–79. [[CrossRef](#)]
4. Lentile, L.; Holden, Z.; Smith, A.; Falkowski, M.; Hudak, A.; Morgan, P.; Lewis, S.; Gessler, P.; Benson, N. Remote sensing techniques to assess active fire characteristics and post-fire effects. *Int. J. Wildland Fire* **2006**, *15*, 319–345. [[CrossRef](#)]
5. Veraverbeke, S.; Dennison, P.; Gitas, I.; Hulley, G.; Kalashnikova, O.; Katagis, T.; Kuai, L.; Meng, R.; Roberts, D.; Stavros, N. Hyperspectral remote sensing of fire: State-of-the-art and future perspectives. *Remote Sens. Environ.* **2018**, *216*, 105–121. [[CrossRef](#)]
6. Tane, Z.; Roberts, D.; Veraverbeke, S.; Casas, A.; Ramirez, C.; Ustin, S. Evaluating endmember and band selection techniques for Multiple Endmember Spectral Mixture Analysis using post-fire imaging spectroscopy. *Remote Sens.* **2018**, *10*, 389. [[CrossRef](#)]
7. Veraverbeke, S.; Stavros, E.N.; Hook, S.J. Remote Sensing of Environment Assessing fire severity using imaging spectroscopy data from the Airborne Visible/Infrared Imaging Spectrometer (AVIRIS) and comparison with multispectral capabilities. *Remote Sens. Environ.* **2014**, *154*, 153–163. [[CrossRef](#)]
8. Dennison, P.E.; Roberts, D.A. Daytime fire detection using airborne hyperspectral data. *Remote Sens. Environ.* **2009**, *113*, 1646–1657. [[CrossRef](#)]
9. Waigl, C.F.; Prakash, A.; Stuefer, M.; Verbyla, D.; Dennison, P. Fire detection and temperature retrieval using EO-1 Hyperion data over selected Alaskan boreal forest fires. *Int. J. Appl. Earth Obs.* **2019**, *81*, 72–84. [[CrossRef](#)]
10. Robichaud, P.R.; Lewis, S.A.; Laes, D.Y.M.; Hudak, A.T.; Kokaly, R.F.; Zamudio, J.A. Postfire soil burn severity mapping with hyperspectral image unmixing. *Remote Sens. Environ.* **2007**, *108*, 467–480. [[CrossRef](#)]
11. Haest, B.; Schepers, L.; Veraverbeke, S.; Spanhove, T.; Borre, J.V.; Kempeneers, P.; Goossens, R. Burn severity assessment of a heathland fire in Belgium using apex hyperspectral indices. In Proceedings of the 9th EARSeL Forest Fire Special Interest Group Workshop, Leicester, UK, 15–17 October 2013.
12. Fernández-Manso, A.; Quintano, C.; Roberts, D.A. Burn severity analysis in Mediterranean forests using maximum entropy model trained with EO-1 Hyperion and LiDAR data. *ISPRS J. Photogram. Remote Sens.* **2019**, *155*, 102–118. [[CrossRef](#)]
13. Escuin, S.; Navarro, R.; Fernández, P. Fire severity assessment by using NBR (Normalized Burn Ratio) and NDVI (Normalized Difference Vegetation Index) derived from LANDSAT TM/ETM images. *Int. J. Remote Sens.* **2008**, *29*, 1053–1073. [[CrossRef](#)]
14. Gitelson, A.A.; Gritz, Y.; Merzlyak, M. Relationships between leaf chlorophyll content and spectral reflectance and algorithms for non-destructive chlorophyll assessment in higher plant leaves. *J. Plant Physiol.* **2003**, *160*, 271–282. [[CrossRef](#)] [[PubMed](#)]
15. Fernández-Manso, A.; Fernández-Manso, O.; Quintano, C. SENTINEL-2A red-edge spectral indices suitability for discriminating burn severity. *Int. J. Appl. Earth Obs.* **2016**, *50*, 170–175. [[CrossRef](#)]
16. Gitelson, A.; Merzlyak, M. Spectral reflectance changes associated with autumn senescence of *Aesculus Hippocastanum* L. and *Acer Platanoides* L. leaves. *J. Plant Physiol.* **1994**, *143*, 286–292. [[CrossRef](#)]
17. Chuvieco, E.; Riaño, D.; Danson, F.M.; Martín, P. Use of radiative transfer model to simulate to postfire spectral response to burn severity. *J. Geophys. Res.* **2006**, *111*, G04S09. [[CrossRef](#)]
18. Pérez-Rodríguez, L.A.; Quintano, C.; García-Llamas, P.; Fernández-García, V.; Taboada, A.; Fernández-Guisuraga, J.M.; Marcos, E.; Suárez-Seoane, S.; Calvo, L.; Fernández-Manso, A. Using Unmanned Aerial Vehicles (UAV) for forest damage monitoring in south-western Europe. In *Imaging Spectrometry XXIII: Applications, Sensors, and Processing*; SPIE: Bellingham, WA, USA, 2019.
19. Filipponi, F. BAIS2: Burned Area Index for Sentinel-2. *Proceedings* **2018**, *2*, 364. [[CrossRef](#)]
20. Boschetti, L.; Roy, D.P.; Justice, C.O.; Humber, M.L. MODIS–Landsat fusion for large area 30m burned area mapping. *Remote Sens. Environ.* **2015**, *161*, 27–42. [[CrossRef](#)]
21. Giglio, L.; Boschetti, L.; Roy, D.P.; Humber, M.L.; Justice, C.O. The collection 6 MODIS burned area mapping algorithm and product. *Remote Sens. Environ.* **2018**, *217*, 72–85. [[CrossRef](#)]
22. Schroeder, W.; Oliva, P.; Giglio, L.; Csiszar, I.A. The New VIIRS 375m active fire detection data product: Algorithm description and initial assessment. *Remote Sens. Environ.* **2014**, *143*, 85–96. [[CrossRef](#)]
23. Phillips, S.J.; Anderson, R.P.; Schapire, R.E. Maximum entropy modeling of species geographic distributions. *Ecol. Model.* **2006**, *190*, 231–259. [[CrossRef](#)]



24. Phillips, S.J.; Anderson, R.P.; Dudík, M.; Schapire, R.E.; Blair, M. Opening the black box: An open-source release of Maxent. *Ecography* **2017**, *40*, 887–893. [[CrossRef](#)]
25. Elith, J.; Graham, C.H. Do they? How do they? WHY do they differ? On finding reasons for differing performances of species distribution models. *Ecography* **2009**, *32*, 66–77. [[CrossRef](#)]
26. Monterroso, P.; Brito, J.C.; Ferreras, P.; Alves, P.C. Spatial ecology of the European wildcat in a Mediterranean ecosystem: Dealing with small radio-tracking datasets in species conservation. *J. Zool.* **2009**, *279*, 27–35. [[CrossRef](#)]
27. Rodríguez-Veiga, P.; Saatchi, S.; Tansey, K.; Balzter, H. Magnitude, spatial distribution and uncertainty of forest biomass stocks in Mexico. *Remote Sens. Environ.* **2016**, *183*, 265–281. [[CrossRef](#)]
28. Park, N.-W. Using maximum entropy modeling for landslide susceptibility mapping with multiple geoenvironmental data sets. *Environ. Earth Sci.* **2015**, *73*, 937–949. [[CrossRef](#)]
29. Amici, V.; Marcantonio, M.; La Porta, N.; Rocchini, D. A multi-temporal approach in MaxEnt modelling: A new frontier for land use/land cover change detection. *Ecol. Inform.* **2017**, *40*, 40–49. [[CrossRef](#)]
30. Arnold, J.D.; Brewer, S.C.; Dennison, P.E. Modeling climate-fire connections within the Great basin and Upper Colorado river basin, Western United State. *Fire Ecol.* **2014**, *10*, 64–75. [[CrossRef](#)]
31. Fonseca, M.G.; Aragao, L.E.O.C.; Lima, A.; Shimabukuro, Y.E.; Arai, E.; Anderson, L.O. Modelling fire probability in the Brazilian Amazon using the maximum entropy method. *Int. J. Wildland Fire* **2016**, *25*, 955–969. [[CrossRef](#)]
32. Quintano, C.; Fernández-Manso, A.; Calvo, L.; Roberts, D.A. Vegetation and Soil Fire Damage Analysis Based on Species Distribution Modeling Trained with Multispectral Satellite Data. *Remote Sens.* **2019**, *11*, 1832. [[CrossRef](#)]
33. Hastie, T.J.; Tibshirani, R.J.; Friedman, J. *The Elements of Statistical Learning*; Springer: Dordrecht, The Netherlands, 2009.
34. Valdecantos, A.; Fuentes, D.; Alloza, J.A.; Vallejo, R. *Report on the Impact of the Carcaixent Forest Fire*; CEAM Foundation-Forestry Program: Valencia, Spain, 2016.
35. Rouse, J.; Haas, R.; Schell, J.; Deering, D. Monitoring Vegetation Systems in the Great Plains with ERTS. In Proceedings of the Third ERTS Symposium, Washington, DC, USA, 10–14 December 1973; pp. 309–317.
36. Birth, G.; McVey, G. Measuring the Color of Growing Turf with a Reflectance Spectrophotometer. *Agron. J.* **1968**, *60*, 640–643. [[CrossRef](#)]
37. Lobell, D.; Asner, G. Hyperion studies of crop stress in Mexico. In Proceedings of the 12th Annual JPL Airborne Earth Science Workshop, Pasadena, CA, USA, 24–28 February 2003.
38. Vogelmann, J.; Rock, B.; Moss, D. Red edge spectral measurements from sugar maple leaves. *Int. J. Remote Sens.* **1993**, *14*, 1563–1575. [[CrossRef](#)]
39. Curran, P.; Windham, W.; Gholz, H. Exploring the Relationship Between Reflectance Red Edge and Chlorophyll Concentration in Slash Pine Leaves. *Tree Physiol.* **1995**, *15*, 203–206. [[CrossRef](#)] [[PubMed](#)]
40. Gao, B. Normalized Difference Water Index for Remote Sensing of Vegetation Liquid Water from Space. In Proceedings of the SPIE'S 1995 Symposium on OE/Aerospace Sensing and Dual Use Photonics, Orlando, FL, USA, 17–21 April 1995; pp. 225–236.
41. Hardisky, M.; Klemas, V.; Smart, R. The Influences of Soil Salinity, Growth Form, and Leaf Moisture on the Spectral Reflectance of Spartina Alterniflora Canopies. *Photogramm. Eng. Remote Sens.* **1983**, *49*, 77–83.
42. Hunt, E., Jr.; Rock, B. Detection of Changes in Leaf Water Content Using Near- And Middle-Infrared Reflectances. *Remote Sens. Environ.* **1989**, *30*, 43–54.
43. Serrano, L.; Penuelas, J.; Ustin, U. Remote Sensing of Nitrogen and Lignin in Mediterranean Vegetation from AVIRIS Data: Decomposing Biochemical from Structural Signals. *Remote Sens. Environ.* **2002**, *81*, 355–364. [[CrossRef](#)]
44. Merzlyak, M.; Gitelson, A.; Chivkunova, O.; Rakitin, V. Non-destructive optical detection of pigment changes during leaf senescence and fruit ripening. *Physiol. Plant.* **1999**, *106*, 135–141. [[CrossRef](#)]
45. Penuelas, J.; Filella, I.; Gamon, J. Assessment of photosynthetic radiation-use efficiency with spectral reflectance. *New Phytol.* **1995**, *131*, 291–296. [[CrossRef](#)]
46. Gamon, J.; Surfus, J. Assessing leaf pigment content and activity with a reflectometer. *New Phytol.* **1999**, *143*, 105–117. [[CrossRef](#)]
47. López-García, M.J.; Caselles, V. Mapping Burns and Natural Reforestation using Thematic Mapper Data. *Geocarto Int.* **1991**, *6*, 31–37. [[CrossRef](#)]

48. Arpacı, A.; Malowerschnig, B.; Sass, O.; Vacik, H. Using multi variate data mining techniques for estimating fire susceptibility of Tyrolean forests. *Appl. Geogr.* **2014**, *53*, 258–270. [[CrossRef](#)]
49. Vilar, L.; Gómez, I.; Martínez-Vega, J.; Echavarría, P.; Riaño, D.; Martín, M.P. Multitemporal modelling of socio-economic wildfire drivers in central Spain between the 1980s and the 2000s: Comparing generalized linear models to machine learning algorithms. *PLoS ONE* **2016**, *11*, e0161344. [[CrossRef](#)] [[PubMed](#)]
50. Bradley, A.P. The use of the area under the ROC curve in the evaluation of machine learning algorithms. *Pattern Recognit.* **1997**, *30*, 1145–1159. [[CrossRef](#)]
51. Congalton, R.G.; Green, K. *Assessing the Accuracy of Remotely Sensed Data PRINCIPLES and Practices*, 2nd ed.; CRC Press, Taylor & Francis: Boca Raton, FL, USA, 2009.
52. Swets, J.A. Measuring the accuracy of diagnostic systems. *Science* **1988**, *240*, 1285–1293. [[CrossRef](#)] [[PubMed](#)]
53. Huang, H.; Roy, D.; Boschetti, L.; Zhang, H.; Yan, L.; Kumar, S.; Gómez-Dans, J.; Li, J. Separability Analysis of Sentinel-2A Multi-Spectral Instrument (MSI) data for Burned Area discrimination. *Remote Sens.* **2016**, *8*, 873. [[CrossRef](#)]
54. Quintano, C.; Fernández-Manso, A.; Fernández-Manso, O. Combination of Landsat and Sentinel-2 MSI data for initial assessing of burn severity. *Int. J. Appl. Earth Obs.* **2018**, *64*, 221–225. [[CrossRef](#)]
55. García-Llamas, P.; Suárez-Seoane, S.; Fernández-Guisuraga, J.M.; Fernández-García, V.; Fernández-Manso, A.; Quintano, C.; Taboada, A.; Marcos, E.; Calvo, L. Evaluation and comparison of Landsat 8, Sentinel-2 and Deimos-1 remote sensing indices for assessing burn severity in Mediterranean fire-prone ecosystems. *Int. J. Appl. Earth Obs.* **2019**, *80*, 137–144. [[CrossRef](#)]
56. Fraser, R.H.; Li, Z.; Cihlar, J. Hotspot and NDVI Differencing Synergy (HANDS): A new technique for burned area mapping over boreal forest. *Remote Sens. Environ.* **2000**, *74*, 362–376. [[CrossRef](#)]
57. Roy, D.P.; Giglio, L.; Kendall, J.D.; Justice, C.O. Multi-temporal active-fire based burn scar detection algorithm. *Int. J. Remote Sens.* **1999**, *20*, 1031–1038. [[CrossRef](#)]
58. Tansey, K.; Beston, J.; Hoscilo, A.; Page, S.E.; Paredes-Hernández, C.U. Relationship between MODIS fire hot spot count and burned area in a degraded tropical peat swamp forest in Central Kalimantan, Indonesia. *J. Geophys. Res.* **2008**, *113*, D23112. [[CrossRef](#)]
59. Roteta, E.; Bastarrika, A.; Storm, T.; Chuvieco, E. Development of a Sentinel-2 burned area algorithm: Generation of a small fire database for northern hemisphere tropical. *Afr. Remote Sens. Environ.* **2019**, *222*, 1–17. [[CrossRef](#)]
60. Chuvieco, E.; Lizundia-Loiola, J.; Pettinari, M.L.; Ramo, R.; Padilla, M.; Tansey, K.; Mouillot, F.; Laurent, P.; Storm, T.; Heil, A.; et al. Generation and analysis of a new global burned area product based on MODIS 250m reflectance bands and thermal anomalies. *Earth Syst. Sci. Data Discuss* **2018**, *10*, 2015–2031. [[CrossRef](#)]
61. Nenzen, H.K.; Araujo, M.B. Choice of threshold alters projections of species range shifts under climate change. *Ecol. Model.* **2011**, *222*, 3346–3354. [[CrossRef](#)]
62. Vogeler, J.C.; Yang, Z.; Cohen, W.B. Mapping post-fire habitat characteristics through the fusion of remote sensing tools. *Remote Sens. Environ.* **2016**, *173*, 294–303. [[CrossRef](#)]

